The Astrophysical Journal, 690:1424–1431, 2009 January 10 doi:10.1088/0004-637X/690/2/1424

SODIUM-22 FROM SUPERNOVAE: A METEORITE CONNECTION

Sachiko Amari
Laboratory for Space Sciences and the Physics Department, Washington University, St. Louis, MO 63130, USA; sa@wuphys.wustl.edu
Received 2008 April 3; accepted 2008 September 16; published 2008 December 12

ABSTRACT

There are several meteoritic noble gas components whose isotopic abundances are distinctly different from the solar abundance. One of these components, Ne-E(L), is a ^{22}Ne-rich component carried by presolar graphite. Neon-22 is dominantly from the radiogenic decay of ^{22}Na ($T_{1/2}$ = 2.6 a), but it also contains ^{22}Ne produced by ^{14}N(α, γ)^{18}F($e^+\nu$)^{18}O(α, γ)^{22}Ne. The proportions of ^{22}Ne from the two different origins vary with graphite density. Many low-density graphite grains (1.65–1.72 g cm^{-3}) exhibit ^{18}O and ^{28}Si excesses, signatures of supernova origin. We revisited noble gas data on bulk (= aggregates) and single-grain analyses of presolar graphite to better understand the origin of Ne-E(L). We conclude that essentially all ^{22}Ne in low-density graphite grains originated from ^{22}Na produced in the O/Ne zone in supernovae. The initial presence of ^{22}Na in these grains indicates that grains formed within a few years after the supernova explosion. The absence of implanted ^{22}Ne can be explained if the grains and the gas in the ejecta became decoupled when they encountered the reverse shock and sputtering eroded the grains in the outer H-rich zone and in the interstellar medium.

Key words: meteors, meteoroids – supernovae: general

1. INTRODUCTION

Primitive meteorites retain the record of the early solar system and beyond because they have experienced little thermal alteration since they formed 4.6 billion years ago. Noble gas analyses of such meteorites revealed that they contain isotopically anomalous noble gases that define distinct components. They include Xe-HL with excesses in both the light and heavy Xe isotopes (Lewis et al. 1975), *s*-process Xe (Xe-S) with excesses in the even isotopes (Srinivasan & Anders 1978), *s*-process Kr (Kr-S; Srinivasan & Anders 1978; Alaerts et al. 1980), and Ne-E with a large excess in ^{22}Ne (Black & Pepin 1969). Ne-E was discovered when Black & Pepin (1969) analyzed Ne in carbonaceous chondrites using a technique where samples are heated in incremental temperature steps ("stepwise heating") and noble gases are analyzed in each step. Neon released in high-temperature steps (900°C–1100°C) was found to be enriched in ^{22}Ne. This new component was named Ne-E because letters from A to D had already been used for the other common Ne components. An upper limit of the ^{20}Ne/^{22}Ne ratio of Ne-E ($\leqslant$ 3.4) set by Black & Pepin (1969) became even lower in subsequent studies (Eberhardt 1974; Eberhardt et al. 1979, 1981; Jungck 1982), prompting the idea that Ne-E was pure ^{22}Ne from the decay of ^{22}Na ($T_{1/2}$ = 2.6 a) (Clayton 1975). Furthermore, these studies indicate that there are two kinds of Ne-E: Ne-E(H) is released in higher-temperature steps (1200°C–1400°C) and is concentrated in higher-density mineral separates (3–3.5 g cm^{-3}), whereas Ne-E(L) is released in lower-temperature steps (500°C–700°C) and is concentrated in lower-density separates ($<$ 2.3 g cm^{-3}; for the details of the discovery of the noble gas components, see Anders (1988)).

The quest for the minerals that contain these anomalous noble gas components ultimately led to the discovery of presolar grains (Lewis et al. 1987; Bernatowicz et al. 1987; Tang & Anders 1988; Amari et al. 1990). Presolar grains are defined as dust that formed in stellar outflows or in stellar ejecta prior to the formation of the solar system, and were subsequently incorporated in primitive meteorites. Diamond, the carrier of Xe-HL, is the first mineral type that was isolated from meteorites in 1987 (Lewis et al. 1987). This discovery was followed by the isolation and identification of SiC (Bernatowicz et al. 1987; Tang & Anders 1988), the carrier of Xe-S, Kr-S, and Ne-E(H). Graphite, carrying Ne-E(L), was isolated from meteorites in 1990 (Amari et al. 1990). Interestingly, the carriers of these noble gas components are all carbonaceous. Graphite is the rarest material among the three carbonaceous types of presolar dust, with an abundance of ~1 ppm in the Murchison meteorite (Amari et al. 1994).

The Ne of Ne-E(H) in presolar SiC originated from ^{22}Ne in the He intershell during the convective thermal pulse in asymptotic giant branch (AGB) stars, where ^{22}Ne is produced by ^{14}N(α, γ)^{18}F($e^+\nu$)^{18}O(α, γ)^{22}Ne and marginally destroyed by ^{22}Ne(α, n)^{25}Mg and ^{22}Ne(α, γ)^{26}Mg (Lewis et al. 1990, 1994; Gallino et al. 1990). The makeup of Ne-E(L) is more complex: it is dominantly from ^{22}Na, although part of the ^{22}Ne is produced in the He intershell of AGB stars, and the proportion of Ne of the two different origins depends on density (Amari et al. 1995a). In this paper, we re-examine noble gas data obtained on both bulk samples and single grains of presolar low-density graphite to further access the origin of Ne-E(L).

2. PRESOLAR GRAPHITE

2.1. Isotopic Features of Low-Density Graphite Grains

Presolar graphite exhibits a range of density (1.6–2.2 g cm^{-3}). Four graphite separates extracted from the Murchison meteorite, KE1 (1.6–2.05 g cm^{-3}, $>$ 1 μm), KFA1 (2.05–2.10 g cm^{-3}, $>$ 1 μm), KFB1 (2.10–2.15 g cm^{-3}, $>$ 1 μm) and KFC1 (2.15–2.20 g cm^{-3}, $>$ 1 μm), have been most extensively studied (Amari et al. 1994). KE3 (1.65–1.72 g cm^{-3}, $>$ 2 μm) was further separated from KE1 to reduce the amount of grains of solar-system origin (Amari et al. 1995b). Thus, the characteristics of isotopically anomalous grains are the same in KE1 and KE3. KE3 was used for single-grain analysis, while KE1 was used for bulk noble gas analysis.

An intriguing feature of presolar graphite is that its isotopic and other features depend on density (Amari et al. 1993; Hoppe et al. 1995). Many grains in the lower-density separates KE3 and KFA1 have isotopically heavy C, whereas those in the higher-density separates KFB1 and KFC1 have isotopically light C. It is mainly low-density graphite grains from KE3 that show ^{14}N/^{15}N ratios lower than the atmospheric ratio (272; Travaglio

et al. 1999), while most grains in the other separates have isotopically normal N (Hoppe et al. 1995). (It has been argued that the normal N in many grains is due to the exchange between indigenous N in the grains and normal N (Hoppe et al. 1995).) Low-density graphite grains have higher trace element concentrations than high-density graphite grains from KFC1. The differences seen in the grains from different density separates extend to morphologies. Graphite grains show two morphologies, termed "cauliflower" and "onion" (Hoppe et al. 1995). Grains of the cauliflower type, looking like aggregates of small grains, consist entirely of turbostratic graphite (i.e., graphite with contorted layers having no long-range continuity). Grains of the onion type consist of a core and concentric shells of fairly well graphitized carbon (Bernatowicz et al. 1991, 1996). Cauliflower grains are more abundant in the low-density separate (Figures 1 and 2), whereas onion grains are more abundant in the high-density separate KFC1.

Low-density graphite grains from KE3 have been studied in detail using secondary ion mass spectrometry. Due to high trace element concentrations and a relatively large grain size (>2 μm), it is possible to analyze isotopic ratios of several elements in the same graphite grains (Amari et al. 1995b, 1996; Travaglio et al. 1999). Many grains have ^{18}O excesses (^{18}O/^{16}O up to 185 times solar). Silicon isotopic anomalies are also observed in these grains, mostly in the form of ^{28}Si excesses, although some grains have ^{29}Si and/or ^{30}Si excesses. They also have high inferred ^{26}Al/^{27}Al ratios up to 0.1. A few grains exhibit ^{44}Ca excesses, the evidence that ^{44}Ti ($T_{1/2} = 60$ a) was once present in the grains (Nittler et al. 1995; Travaglio et al. 1999).

The isotopic features of low-density graphite grains are similar to those of SiC grains of type X (Amari et al. 1992; Nittler et al. 1995; Hoppe et al. 2000). Silicon-28 excesses and the presence of ^{44}Ti in both types of grains indicate that they formed in supernovae: ^{28}Si is produced in the O-burning zone in Type II supernovae, and ^{44}Ti is produced only by explosive nucleosynthesis, the strongest proof of their supernova origin. Other isotopic features of the graphite grains can be traced back to different zones of supernovae. Oxygen-18 is produced in the He/C zone via ^{14}N(α, γ)^{18}F($e^+\nu$)^{18}O (names of the zones, coined by Meyer et al. (1995), indicate most abundant elements), where partial He burning takes place. Aluminum-26 is produced via ^{25}Mg(p, γ)^{26}Al in the He/N zone, where the CNO cycle occurs. However, since predicted isotopic anomalies in these zones from supernova models are much higher than those observed in these grains, it requires mixing in different zones to reproduce the isotopic ratios of these grains. We note that the He/C and He/N zones are the only C-rich zones in supernovae. Carbon monoxide (CO) being one of the most stable molecules, C > O is required to have free C to form carbonaceous grains. Clayton et al. (1999) proposed that in supernova ejecta carbonaceous grains form even under the O-rich environment: energetic electrons produced by radioactive isotopes dissociate CO molecules and free C atoms to form carbonaceous dust. And the association of C atoms takes place faster than the dissociation by oxidation. It remains to be seen whether or not carbonaceous grains form and grow in the O-rich supernova ejecta. We note, however, that material from the outer C-rich zones is required to explain several isotopic features of the grains including that of C, the major element of graphite.

To quantitatively evaluate whether the low-density graphite data can be explained with supernova models, Travaglio et al. (1999) calculated mixing between different zones of supernovae, using one-dimensional supernova models by Woosley & Weaver (1995). They concluded that the mixing model can explain the observed C and Si isotopic ratios as well as ^{18}O/^{16}O ratios and the initial presence of ^{44}Ti if jets of material in the inner Si-rich zones are assumed to penetrate the huge O-rich zones and are ejected into and mixed with the outer C-rich zones. Thus, grains that bear these isotopic features, namely ^{28}Si and ^{18}O excesses as well as the initial presence of ^{44}Ti, most likely formed in supernova ejecta. This scenario requires small-scale mixing of the ejecta.

With mixing elements in different zones in consideration, Clayton et al. (2002) investigated the formation of SiC X grains and their subsequent interactions with the gas to explain isotopic compositions of Fe. They proposed that when SiC grains, formed in the inner Si/S zone, encounter the reverse shock, they move forward with the velocity of about a few hundred km s^{-1}. Atoms in the outer zones would be implanted into the depths of 0.04–0.1 μm. Iron condensed into the grains is mixed with Fe implanted in the grains. As a result, isotopic ratios of SiC X grains reflect mixing of trace elements from different nucleosynthetic zones.

Marhas et al. (2008) analyzed Fe and Ni isotopic ratios in SiC X grains and argued that their results do not support the scenario proposed by Clayton et al. (2002). Most of the Fe and Ni in their grains originate from the zones with close-to-solar isotopic compositions; thus elemental ratios of Fe, Co, and Ni are also expected to be close to solar if they were implanted. However, the abundances of Co and Ni relative to Fe are much higher than solar. This is contrary to what is expected from implantation which would not differentiate those elements. Another point they raised is that Fe as well as Co and Ni are not confined to the surface of the grains, but are present throughout the grains (average grain size: ~ 3 μm) although their concentrations vary.

Even though implantation cannot account for the Fe isotopic ratios in the SiC X grains, it may work for other elements. For example, Kr-S in the separates KE1 + KFA1 indicates a massive star origin (see below). In this case, implantation is the only possible mechanism for grains to acquire their noble gases.

2.2. Noble Gas Data for Graphite

Amari et al. (1995a) analyzed four noble gases (all except He) from bulk samples of KE1, KFA1, KFB1, and KFC1 by stepwise heating and found that although a dominant source of ^{22}Ne in Ne-E(L) is ^{22}Na, a portion of the ^{22}Ne originated from ^{22}Ne in the He intershell during the convective thermal pulse in AGB stars. Furthermore, the proportions of ^{22}Ne of the two different origins vary among the separates. Since Ne compositions of the He intershell in AGB stars vary slightly with their mass and metallicity, the estimated proportions of the ^{22}Ne of the two different origins vary depending on mass (1–3 $M_{\rm sun}$) and metallicity ($Z = 0.002$–0.02, $Z_{\rm solar} = 0.02$) of AGB stars: about 94–95% of the ^{22}Ne is from ^{22}Na in KE1, 84–90% in KFA1, 49–76% in KFB1, and 82–87% in KFC1 (Amari et al. 1995a).

Kr-S was observed in all the separates (Amari et al. 1995a). ^{86}Kr and ^{80}Kr abundances are sensitive to nucleosynthetic conditions in stars. Krypton-85 on the s-process path decays to ^{85}Rb with the half-life of 11 years. Thus, the ^{86}Kr abundance depends on the neutron density. Selenium-79 is at a branching point of the s-process and its behavior is critical to ^{80}Kr yields. The half-life of ^{79}Se strongly depends on temperature: it is much shorter under stellar conditions (one month at $\sim 1 \times 10^9$ K) than

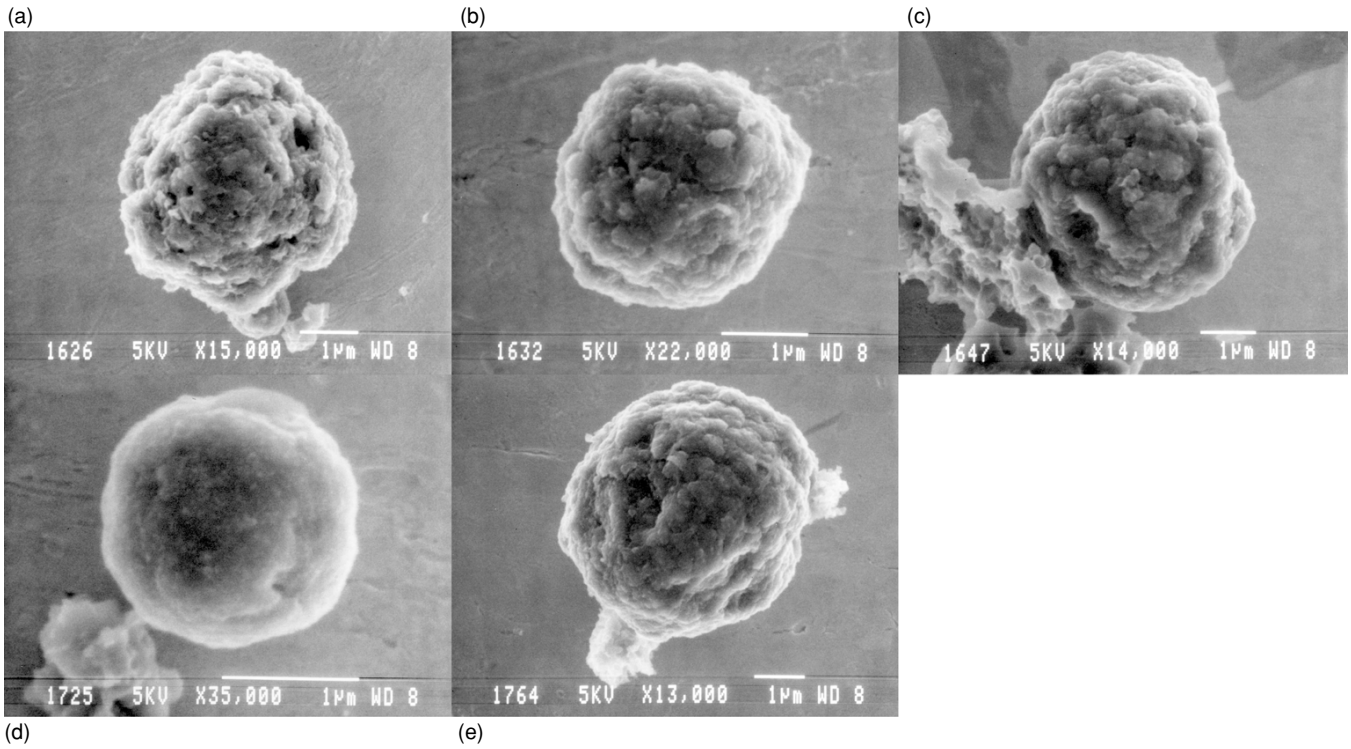

Figure 1. SEM secondary electron images of the ^{22}Ne-rich grains from separate KE3 before the analysis. They are typical grains of the cauliflower type (see text). Scale bars are 1 μm. (a) KE3a-155, (b) KE3a-172, (c) KE3a-244, (d) KE3a-573, and (e) KE3a-751. Fluffy grains on the lower left in (c) and (e) are most likely of solar system origin.

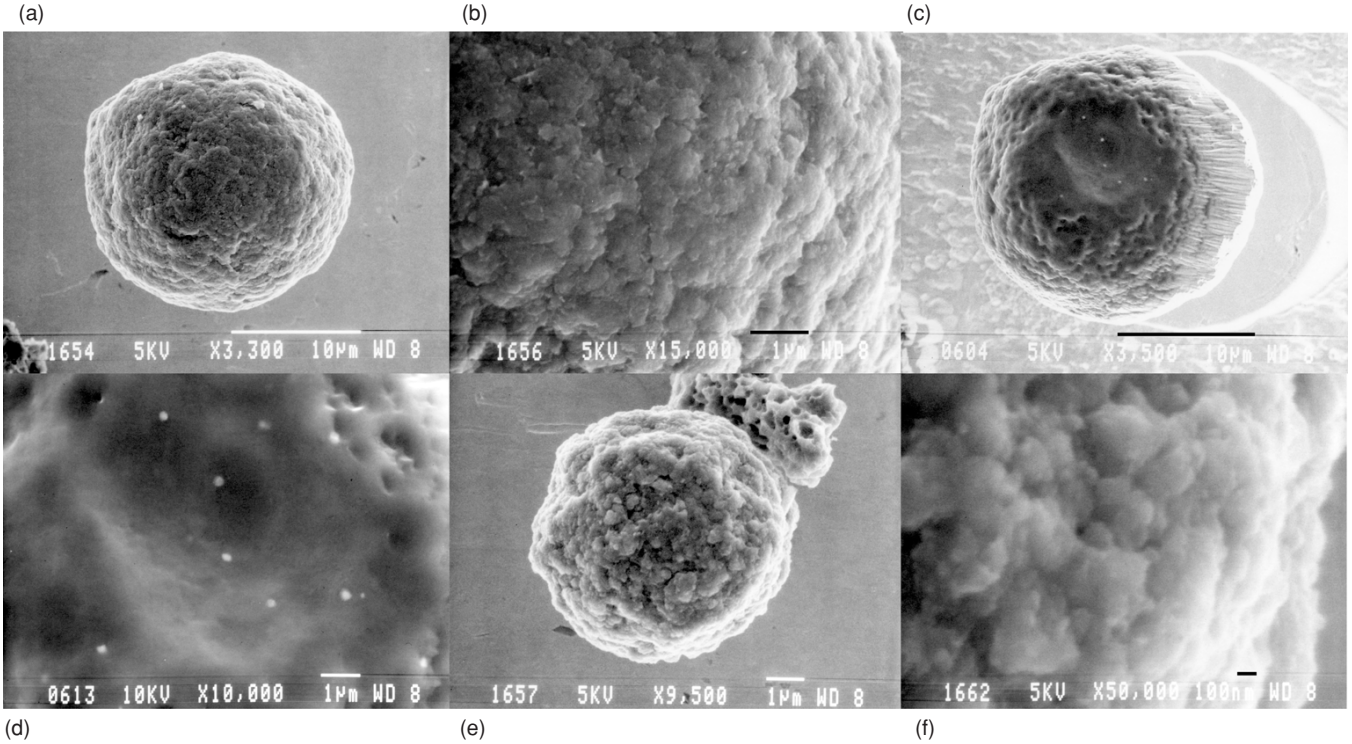

Figure 2. SEM secondary electron images of the ^{22}Ne-rich grains from separate KE3 before the analysis ((a), (b), (e), and (f)) and after the ion probe analysis ((c) and (d)). Scale bars are 10 μm in (a) and (c), 1 μm in (b), (d) and (e), and 100 nm in (f). (a) KE3a-321. (b) Detailed surface structure of KE3a-321. (c) KE3a-321 after the ion probe analysis. The grain sits on a pedestal because the gold substrate around the grain was sputtered faster than the grain. After the sputtering of the grain by the ion probe, TiC subgrains (small white spots in the grain), originally inside the graphite grain, appear on the surface of the graphite grain. (d) A magnified picture of the TiC subgrains in KE3a-321. (e) KE3a-322. The grain attached to grain KE3a-322 in the upper right is most likely of solar system origin. (f) Detailed surface structure of KE3a-322.

in terrestrial conditions (650,000 years; Klay & Käppeler 1988). As a consequence, ^{80}Kr abundances depend on both neutron density and temperature.

Interestingly, the *s*-process ^{86}Kr/^{82}Kr ratio of KFC1 and that of the separates KE1 and KFA1 are completely different (see Figures 3 and 5 in Amari et al. (1995a)). The *s*-process ^{86}Kr/^{82}Kr and ^{80}Kr/^{82}Kr ratios were derived assuming that the *s*-process ^{83}Kr/^{82}Kr ratio was 0.3 (Amari et al. 1995a). (The ^{83}Kr/^{82}Kr ratio was used to infer other Kr-S isotopic ratios because it is predicted to be constant and defined by the inverse ratio of their neutron capture cross sections at relatively low temperature ($kT \sim 30$ keV).) Kr-S in the highest-density separate KFC1 points toward low-metallicity ($Z \leqslant 0.002$) AGB stars. The Kr-S in the lower-density separates was first attributed to high-metallicity ($Z \geqslant 0.025$) AGB stars (Amari et al. 1995a). Recently, it has been proposed that the Kr-S in the lower-density separates was produced in massive stars (Amari et al. 2006). Using supernova models by Chieffi & Limongi (2004) and updated calculations of nucleosynthetic yields in AGB stars (R. Gallino 2005, private communication), Amari et al. (2006) recalculated the *s*-process ^{86}Kr/^{82}Kr and ^{80}Kr/^{82}Kr ratios of these Murchison graphite separates: the *s*-process ^{86}Kr/^{82}Kr and ^{80}Kr/^{82}Kr ratios for KFC1 are 4.43 ± 0.46 and 0.030 ± 0.047, respectively, assuming *s*-process ^{83}Kr/^{82}Kr = 0.375 instead of 0.3, reflecting the improvement of precision of analyses in neutron capture cross sections. Those for KE1+KFA1 are 0.02 ± 0.26 and 0.070 ± 0.045, respectively, assuming *s*-process ^{83}Kr/^{82}Kr = 0.334 (predicted in the O/C zone in a 25 $M_{\rm sun}$ star with solar metallicity), and 0.67 ± 0.14 and 0.127 ± 0.023, respectively, with ^{83}Kr/^{82}Kr = 0.623 (predicted in the O/Ne zone). A difficulty in inferring *s*-process ratios in massive stars is that *s*-process ^{83}Kr/^{82}Kr ratios, which are needed to infer *s*-process ^{86}Kr/^{82}Kr and ^{80}Kr/^{82}Kr ratios, depend on neutron capture cross sections of the both isotopes, and that of ^{83}Kr deviates from the classical $1/v$ rule (v: thermal velocity) at high temperature ($\sim 10^9$ K). Thus, ^{83}Kr/^{82}Kr ratios at high temperatures have a greater uncertainty. It remains to be seen whether supernova models can fully account for the Kr-S in the lower-density separates.

Helium-4 and ^{20,22}Ne in single graphite grains from KE3 (Nichols et al. 1994), KFB1 (Nichols et al. 1992), and KFC1 (Kehm et al. 1996) were analyzed. Grains suspended in a mixture of isopropanol and water were deposited onto a gold foil. After examining grains for their chemical composition, size, and morphology with the scanning electron microscope (SEM), they were analyzed for their isotopic ratios with the CAMECA-3f at Washington University. KFB1 and KFC1 grains were analyzed for their C and N isotopic ratios. KE3 grains were analyzed for their C, N, Al–Mg, O, and Si isotopic ratios. Calcium and Ti isotopic ratios were also measured for two of the KE3 grains (Tables 1 and 2). The grain sizes were again determined with the SEM prior to the noble gas analyses. The grains were subsequently vaporized with a neodymium-doped yttrium aluminum garnet (Nd:YAG) laser and ^{4}He and ^{20,22}Ne were analyzed by the high-sensitivity noble gas mass spectrometer (Hohenberg 1980). In all measured grains from KE3, KFB1, and KFC1, ^{4}He and ^{20}Ne were under detection limits. Not all the grains are ^{22}Ne-rich, and the fractions of ^{22}Ne-rich grains vary among the separates (KE3: 9 out of 21, KFB1: 14 out of 51, and KFC1: 3 out of 46). We note that Heck et al. (2008) recently analyzed 51 KFB1 grains with known ^{12}C/^{13}C and ^{18}O/^{16}O ratios and found that 11 grains contained measurable ^{22}Ne; of these 11 grains one grain had ^{20}Ne and ^{4}He and another grain had ^{20}Ne. Results of ion probe and noble gas analyses in KE3 gains are summarized in Tables 1 and 2. Secondary electron images of the KE3 grains taken with the SEM are shown in Figures 1 and 2.

3. DISCUSSION

3.1. The Origin of ^{22}Ne in Low-Density Graphite

In this paper, we focus on low-density graphite grains from the separates KE1 and KE3. Of the nine ^{22}Ne-rich grains in KE3, eight grains were analyzed for their C, N, O, Al–Mg, and Si isotopic ratios in addition to Ca and Ti isotopic ratios for two of the grains prior to the noble gas analysis (Tables 1 and 2). ^{12}C/^{13}C ratios of these grains range from 27 to 153 (solar: 89; Figure 3(a)). Six out of eight grains show isotopically heavy N (^{14}N/^{15}N ratios down to 110, air: 272). ^{26}Al/^{27}Al ratios of four grains are in the range of 10^{-2}, two in the range of 0.1 with the highest ratio of 0.125 ± 0.001. Although errors of the ^{17}O/^{16}O ratios are large due to the low abundance of ^{17}O, grain KE3a-321 has an ^{17}O excess, grain KE3a-573 a deficit. Seven out of eight grains show elevated ^{18}O/^{16}O ratios (6.83×10^{-3} to 0.119) above the solar ratio (2×10^{-3}). Grain KE3a-573 shows a normal ^{18}O/^{16}O ratio, but has a ^{28}Si excess (Figure 3). Seven grains have Si isotopic anomalies: five grains with ^{28}Si excesses, one with ^{29}Si excess, and one with both ^{29}Si and ^{30}Si excesses (Figure 3(b)). Furthermore, grains KE3a-321 and KE3a-322 show the initial presence of ^{44}Ti. Since all eight grains show either ^{18}O excesses and/or ^{28}Si excesses, the signatures of supernova grains, we conclude that all of the eight ^{22}Ne-rich grains formed in supernovae.

Particularly interesting is grain KE3a-573 (Figure 1(d)). Due to its high ^{22}Ne content, Nichols et al. (1994) were able to set an upper limit of 0.01 on its ^{20}Ne/^{22}Ne ratio. In supernova models, the lowest ^{20}Ne/^{22}Ne ratio is found in the He/C zone, a partial He-burning zone where ^{22}Ne is produced via ^{14}N(α, γ)^{18}F($e^+\nu$)^{18}O(α, γ)^{22}Ne. Predicted ^{20}Ne/^{22}Ne ratios are 0.096 (Rauscher et al. 2002) and 0.088 (Chieffi & Limongi 2004) in a 25 $M_{\rm sun}$ star with solar metallicity. These ratios are well above the upper limit of the ^{20}Ne/^{22}Ne of grain KE3a-573, indicating that the ^{22}Ne in the grain originated from another source.

Sodium-22 is produced in the O/Ne zone during hydrostatic C burning (see Section 3.2) (Rauscher et al. 2002; Chieffi & Limongi 2004). This is the only ^{22}Ne source in supernovae that satisfies the observed ^{20}Ne/^{22}Ne upper limit. In this zone the predicted ^{20}Ne/^{22}Ne and ^{20}Ne/^{22}Na ratios are 480 and 1.13×10^5 (Rauscher et al. 2002), and 1140 and 1.03×10^5 (Chieffi & Limongi 2004), respectively. Any addition of Ne to ^{22}Na in the zone will dramatically raise the ^{20}Ne/^{22}Ne ratio; thus ^{22}Na alone is needed to account for the observed ^{22}Ne in grain KE3a-573. Even if ^{22}Na is added to ^{22}Ne in the He/C zone, where the lowest ^{20}Ne/^{22}Ne ratio is predicted, the lower upper limit of the grain cannot be explained: the abundance of ^{22}Na in the O/Ne zone is more than three orders of magnitude lower than that of ^{22}Ne in the He/C zone (^{22}Na$_{\rm O/Ne}$/^{22}Ne$_{\rm He/C}$ = 1.07×10^{-4} and 1.60×10^{-4} by Rauscher et al. (2002) and by Chieffi & Limongi (2004), respectively). Therefore, the addition of ^{22}Na does not change the ^{20}Ne/^{22}Ne ratio of the He/C zone. This implies that the ^{22}Ne in the grain is entirely from the decay of ^{22}Na: if Ne was in the grains, a much higher upper limit or a ratio should have been observed.

Since upper limits of the ^{20}Ne/^{22}Ne ratios, or the ratios themselves, for the other seven ^{22}Ne-rich grains were not

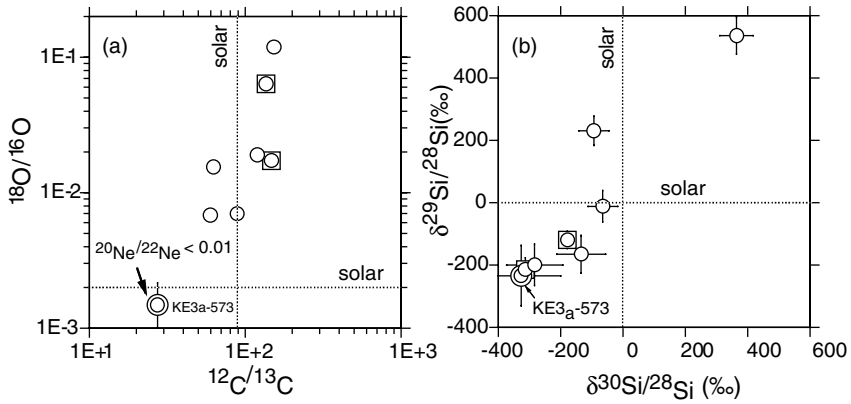

Figure 3. Eight ^{22}Ne-rich low-density graphite grains are plotted for their (a) $^{12}C/^{13}C$ and $^{18}O/^{16}O$ ratios and (b) Si isotopic ratios. The Si isotopic ratios are expressed with delta values that represent deviations from the solar ratios by a thousand. Grain KE3a-573, shown with the double circle, has an upper limit in its $^{20}Ne/^{22}Ne$ ratio. Two grains marked with the square show the evidence of ^{44}Ti.

Table 1
Neon-22 Contents and C, N, Al, and Si Isotopic Compositions of KE3a Grains

Grain	Diameter[a] (μm)	$^{22}Ne \times 10^{-3}$ (cm^3 STP g^{-1})[b]	$^{12}C/^{13}C$	$^{14}N/^{15}N$	$^{17}O/^{16}O\ 10^{-4}$	$^{18}O/^{16}O\ 10^{-3}$	$^{26}Al/^{27}Al\ 10^{-2}$	$^{29}Si/^{28}Si$[c] (‰)	$^{30}Si/^{28}Si$[c] (‰)
KE3a-155	4.0 (2.1)	1.2 ± 0.7	62.5 ± 0.7	240 ± 8	n.m.	15.5 ± 2.5	8.87 ± 0.16	−165 ± 60	−135 ± 78
KE3a-172	2.7 (1.4)	4.2 ± 2.1	59.7 ± 0.9	149 ± 9	3.01 ± 0.85	6.83 ± 0.68	4.18 ± 0.19	−200 ± 66	−284 ± 90
KE3a-244	4.4 (2.1)	1.5 ± 0.6	88.7 ± 0.9	267 ± 6	4.21 ± 0.72	6.99 ± 0.49	0.89 ± 0.12	−12 ± 50	−66 ± 47
KE3a-321	20 (10.3)	0.02 ± 0.01	135.9 ± 1.0	215 ± 10	10.9 ± 2.3	63.6 ± 3.2	10.37 ± 0.11	−214 ± 37	−314 ± 33
KE3a-322	6.8 (3.0)	1.9 ± 0.2	147.2 ± 1.8	161 ± 8	3.80 ± 0.45	17.3 ± 0.5	12.5 ± 0.1	−120 ± 27	−179 ± 17
KE3a-563	4.4 (2.4)	7.0 ± 0.7	119.4 ± 3.8	191 ± 7	3.58 ± 0.83	19.0 ± 1.0	1.27 ± 0.07	536 ± 59	364 ± 53
KE3a-573	1.8 (0.9)	13.2 ± 8.1	27.3 ± 0.3	259 ± 17	0.9 ± 1.0	1.48 ± 0.67		−235 ± 97	−327 ± 128
KE3a-751	4.7 (2.3)	0.5 ± 0.4	152.7 ± 3.5	110 ± 8	2.46 ± 0.90	119 ± 4	4.70 ± 0.07	230 ± 47	−94 ± 48
KE3a-099	(2.9)	6.7 ± 0.5	n.m.	n.m.	n.m.	n.m.	n.m.	n.m.	n.m.
Solar			89	272[d]	3.83	2.01		0	0

Notes.
[a] Diameter before (without a parenthesis) and after (with a parenthesis) the ion probe analysis.
[b] cm^3 in standard temperature and pressure per gram.
[c] $^{i}Si/^{28}Si$ (‰) $\equiv [(^{i}Si/^{28}Si)_{grain}/(^{i}Si/^{28}Si)_{solar} - 1] \times 1000$.
[d] The atmospheric ratio.
Data in Tables 1 and 2 are from Nichols et al. (1994) and Travaglio et al. (1999).
Errors in Tables 1 and 2 are 1σ.

Table 2
Calcium and Ti Isotopic Compositions of KE3a Grains

Grain	$\delta^{42}Ca/^{40}Ca$ (‰)	$\delta^{43}Ca/^{40}Ca$ (‰)	$\delta^{44}Ca/^{40}Ca$ (‰)	$^{44}Ti/^{48}Ti\ 10^{-3}$	$\delta^{46}Ti/^{48}Ti$ (‰)	$^{47}Ti/^{48}Ti$ (‰)	$^{49}Ti/^{48}Ti$ (‰)
KE3a-321	30 ± 19	72 ± 41	76 ± 14	1.06 ± 0.22	22 ± 11	−5 ± 11	296 ± 13
KE3a-322	34 ± 33	69 ± 57	53 ± 23	2.4 ± 1.1	78 ± 27	−4 ± 26	576 ± 36

Notes.
[i] $Ca/^{40}Ca$ (‰) $\equiv [(^{i}Ca/^{40}Ca)_{grain}/(^{i}Ca/^{40}Ca)_{solar} - 1] \times 1000$.
[i] $Ti/^{48}Ti$ (‰) $\equiv [(^{i}Ti/^{48}Ti)_{grain}/(^{i}Ti/^{48}Ti)_{solar} - 1] \times 1000$.

determined, it is not possible to discern the origin of the ^{22}Ne in these grains solely from the single-grain analysis. However, if we take both the single-grain analysis and the bulk analysis into account, it is possible to determine the origin of ^{22}Ne in these grains. The total $^{20}Ne/^{22}Ne$ and $^{21}Ne/^{22}Ne$ ratios of KE1 from the bulk analysis are 0.0301 ± 0.0018 and 0.000118 ± 0.000017, respectively. We assume that the Ne in KE1 is a three-component mixture: ^{22}Ne from ^{22}Na ($^{20}Ne/^{22}Ne$: 0, $^{21}Ne/^{22}Ne$: 0), solar Ne ($^{20}Ne/^{22}Ne$: 13.7, $^{21}Ne/^{22}Ne$: 0.0333) (Anders & Grevesse 1989) and Ne in the He/C zone, where $^{20}Ne/^{22}Ne$ is the lowest among the supernova zones. If we take the ratios by Rauscher et al. (2002) ($^{20}Ne/^{22}Ne$: 0.09620, $^{21}Ne/^{22}Ne$: 0.007837, 25 M_{sun} with solar metallicity), more than 99% of ^{22}Ne is from ^{22}Na. If we take the ratios by Chieffi & Limongi (2004) ($^{20}Ne/^{22}Ne$: 0.08834, $^{21}Ne/^{22}Ne$: 4.317×10^{-5}, 25 M_{sun} with solar metallicity), due to the very small $^{21}Ne/^{22}Ne$ ratio, the total KE1 ratios plot slightly out of the triangle bound by the three components in a Ne three-isotope plot, and lie very close to the mixing line between ^{22}Na and solar Ne. If we assume a two-component mixing, more than 99% of the ^{22}Ne is from ^{22}Na. Thus, it appears that all eight ^{22}Ne-rich grains having the supernova isotopic signature contain ^{22}Ne solely from the decay of ^{22}Na.

3.2. Stellar Sources of ^{22}Na

Novae have been considered to be a major source of ^{22}Na in Ne-E(L). They are close binary systems consisting of a white dwarf and a companion star. The H-rich envelope material

accretes onto the white dwarf from the companion star, is compressed, and finally a thermonuclear runaway takes place. Depending of the composition of white dwarfs, novae are classified into CO novae and ONe novae. White dwarfs of CO novae are C- and O-rich with mass typically less than 1.1 $M_{\rm sun}$. ONe novae are explosions on O- and Ne-rich white dwarfs that are more massive ($\geqslant 1.1\,M_{\rm sun}$) than CO white dwarfs. ONe novae range a main source of ^{22}Na: ^{22}Na is produced via ^{20}Ne(p, γ)^{21}Na($\beta^+\nu$)^{21}Ne(p, γ)^{22}Na that requires $T \sim 4 \times 10^8$ K. Massive white dwarfs, such as ONe white dwarfs, can reach high peak temperatures close to the above temperature range, and produce a sufficient amount of ^{22}Na. José & Hernanz (1998) show that ^{22}Na yields in ONe novae are more than two orders of magnitude higher than those in CO novae (mass fractions of ^{22}Na in ONe novae range from 3.1 to 65 $\times$ 10^{-5}, while those in CO novae range from 8.5 to 34 $\times$ 10^{-8}). Both types of novae have characteristic ^{20}Ne/^{22}Ne ratios. The higher ^{20}Ne abundances in ONe novae lead to much higher ^{20}Ne/^{22}Ne ratios (37–2890) than those expected in CO novae (0.07–0.72) (José & Hernanz 1998; José et al. 2004). Furthermore, ^{22}Na is produced in the ejecta where Ne is overwhelmingly abundant. ^{22}Na/^{22}Ne ratios of CO novae range from 1.51 $\times$ 10^{-5} to 1.73 $\times$ 10^{-4} and those of ONe novae from 2.40 $\times$ 10^{-2} to 4, indicating that, even if all ^{22}Na is added to ^{22}Ne, resulting ^{20}Ne/^{22}Ne ratios of nova ejecta remain unchanged (José & Hernanz 1998).

As noted in Section 3.1, ^{22}Na is also produced in the O/Ne zone in supernovae during hydrostatic C burning by ^{21}Ne(p, γ)^{22}Na, where ^{21}Ne is produced by ^{20}Ne(n, γ)^{21}Ne and protons by ^{12}C(^{12}C, p)^{23}Na. The mass fraction of ^{22}Na is 1.6 $\times$ 10^{-6} and 3.3 $\times$ 10^{-6} by Rauscher et al. (2002) and Chieffi & Limongi (2004), respectively. It is also the case in supernovae that ^{22}Na is produced in the zone where ^{20}Ne is overwhelmingly (more than five orders of magnitude) abundant than ^{22}Na (see Section 3.1).

The isotopic features of the ^{22}Ne-rich grains and the noble gas data, both on the single grains and the bulk samples, indicate that these low-density graphite grains contain ^{22}Ne solely from the decay of ^{22}Na produced in supernovae. For high-density graphite grains, the origin of ^{22}Na, whether it was produced in supernovae or novae (or both), remains to be determined.

3.3. Sodium-22 in Low-Density Graphite

The presence of initial ^{22}Na in the low-density graphite grains and its short half-life (2.6 a) indicate that the grains formed within a few years after the explosion before ^{22}Na completely decayed to ^{22}Ne. Infrared observations of 1987A indicate that grain formation started around 350 days after the explosion and became rapid at around 500 days (e.g., McCray 1993). The presence of ^{22}Na in the grains is consistent with these observations.

^{22}Na seems to have been incorporated throughout the grains. Prior to the noble gas analysis on single grains, these grains were considerably consumed during the ion probe analysis (Table 1). Despite the loss of the outer portion of the grains, ^{22}Ne was still detectable during the single-grain analysis, indicating that ^{22}Na was distributed throughout the grains. To implant Na into 1 μm depth from the surface, a relative velocity of Na and the grains is $\sim$2200 km s^{-1} (http://www.srim.org/). Bombardment of ions or atoms at such a huge relative velocity for a long period would have eroded the grains. Another reason to exclude implantation as a trapping mechanism of ^{22}Na is that implantation does not differentiate Na and Ne, resulting in too high ^{20}Ne/^{22}Ne ratios in the grains: ^{22}Na is produced in the Ne-rich zone with a high ^{20}Ne/^{22}Ne ratio (see Section 3.1).

Sodium is more likely to be intercalated into graphite. It has been known that many kinds of elements/compounds, including Na, can be intercalated into graphite. Graphite intercalation compounds are characterized by intercalate layers that are periodically arranged in a matrix of graphite layers (for details, see the review paper by Dresselhaus & Dresselhaus (2002)).

The incorporation of ^{22}Na throughout the graphite grains favors the idea that they grew in the O-rich region where ^{22}Na was produced. In fact this is where Clayton et al. (1999) had proposed graphite formation with radioactive isotopes dissociating CO. We know very little about mixing in supernovae during the explosion. One-dimensional and two-dimensional supernova models are not likely to reflect a real sequence of events during the explosion. It is our hope to gain a better understanding on mixing and grain formation when three-dimensional supernova calculations are fully implemented.

3.4. Absence of Implanted Ne

Although ^{20}Ne is five orders of magnitude more abundant than ^{22}Na in the O/Ne zone, implanted Ne is not observed in the graphite grains. Here we will discuss a possible scenario where ^{22}Na was incorporated into the grains unaccompanied by ambient Ne. As discussed previously, ^{22}Na most likely had been intercalated into the grains as they grew in the ejecta. Since Ne is chemically inert, the only way that Ne was incorporated into the grains is ion implantation or atom bombardment. The absence of implanted Ne indicates either relative velocities between the grains and the gas were always zero, or Ne was originally implanted (due to differences of velocities between the grains and the gas) but was subsequently removed. The former is not likely: although relative velocities between the grains and the gas are considered to be small compared with expanding velocities of the supernova ejecta (see below), it is very likely that there are some differences in velocities of the grains and the gas. We consider the latter case and we will first estimate the penetration depth of Ne into the grains, and then evaluate whether or not the Ne in that layer could be preserved subsequently.

Infrared observations of Cassiopeia A with the *Spitzer* Space Telescope have revealed that, along radial lines from the explosion, the nucleosynthetic zones are largely intact, although some degree of mixing occurred (Rho et al. 2008; Rudnick 2008). Those observations also show that nucleosynthetic zones are associated with characteristic dust populations: silicate dust emission is observed where Si, S, and Ar are detected in various wavelengths, implying that the dust formed in the O-burning zone. Al_2O_3 is associated with Ne and O gases, indicative of the C-burning zone. These observations indicate that grains formed in the expanding ejecta. The close association of the nucleosynthetic zones and characteristic dust compositions suggests that dust and the gas move with approximately the same velocity, or that relative velocities between the gas and the grains are small compared with observed velocities of the ejecta.

In fact, laboratory examinations of supernova graphite grains also confirm that this is indeed the case. Croat et al. (2003) examined ultramicrotome slices of 12 low-density graphite grains from KE3 with transmission electron microscopy (TEM). Of them, 10 graphite grains contain TiC subgrains, and less frequently, kamacite (Ni-rich iron) subgrains. The average diameter of the TiC grains range from 30 to 232 nm and their

abundance from 25 to 2400 ppm. These TiC subgrains, randomly distributed in host graphite grains, indicate that the TiC grains formed first and were subsequently incorporated into the host graphite grains. The presence of internal TiC subgrains is also seen in KE3a-321 (Figures 2(c) and 2(d)).

Six to 50% of the TiC grains that Croat et al. (2003) examined have amorphous rims with the thickness of 3–15 nm and these rimmed grains were present in all 10 graphite grains with TiC subgrains. They speculate that these rims are the result of atom bombardment from the surrounding gas. To estimate stopping ranges, or penetration depths, we need to specify gas species impinging into TiC. We considered ^{4}He (most abundant in the outer He-rich zones), ^{16}O (most abundant in the inner O-rich zones), and ^{20}Ne as the gas species and calculated their velocities to penetrate 3–15 nm into TiC grains using the SRIM code (http://www.srim.org/). With ^{20}Ne, the relative velocity ranges from 130 to 350 km s^{-1}. (With ^{4}He, 150 to 370 km s^{-1}, and with ^{16}O, 130 to 360 km s^{-1}.) This is a small fraction of velocities of supernova ejecta (a few thousand km s^{-1}) estimated from observations. For example, from the ultraviolet and optical lines, an expansion velocity of Type IIn SN 1998S was estimated to be ∼7000 km s^{-1} (Fransson et al. 2005). It is difficult to estimate relative velocities of the gas and the host graphite grains in the same manner because the surface of the graphite grains was sputtered by the ion probe prior to the TEM analysis. In addition, low-density graphite grains consist entirely of turbostratic graphite (Bernatowicz et al. 1996) and this makes it hard to evaluate the change of surface crystal structure. If we assume that the relative velocity between the graphite grains and ^{20}Ne is 130–350 km s^{-1}, ^{20}Ne penetrates 6–30 nm into the graphite grains.

When the reverse shock hits the ejecta, the gas and grains become decoupled. Grains, due to larger masses, are much less decelerated than the gas, and keep moving outward into the H-rich region and the interstellar medium (ISM), where the gas is heated with the reverse shock and with the forward shock, respectively. Grains traveling through these places are sputtered by abundant H ions. Nozawa et al. (2007) investigated the evolution of dust in the ejecta when it collides with the reverse shock. They assumed that dust grains in the inner zones are never processed by either kinetic or thermal sputtering before they hit the reverse shock, because the dust grains and the gas move at the same velocity and the gas temperature is too low for thermal sputtering. When the dust grains encounter the reverse shock, decoupling of the gas and the dust grains takes place. Due to the grains' much larger masses, they are not decelerated as much as the gas. Relative velocities depend on various parameters such as masses of grains and expanding speed of the ejecta. The dust grains move into the hot gas (10^{7}–10^{8} K) heated by the reverse shock and the forward shock, causing kinetic and thermal sputtering. Nozawa et al. (2007) simulated the grain history after grains hit the reverse shock with their standard model (M (mass of supernovae) = 20 $M_{\rm sun}$, the H number density in the ISM = 1 cm^{-3}). Carbon grains of 1 μm in diameter lose 0.7%, or 7 nm, of their sizes when they move through the H-rich zone and later into the ISM. This value certainly varies depending on conditions such as initial diameters of the grains. Low-density graphite grains are not perfectly crystallized graphite; thus they are more susceptible to sputtering. Therefore, even if ^{20}Ne was implanted in the ejecta where grains formed, the very thin surface layer where Ne was implanted would likely be sputtered away during the subsequent journey through the H-rich zone into the ISM.

We note that this scenario cannot be applied if Ne was implanted onto the grains throughout grain growth. If so, Ne would have been distributed throughout the grains. It may indicate that the velocity difference between the grains and the gas appeared when grain growth was almost complete.

The origin of ^{22}Na in higher-density graphite grains has not been determined yet. If it was produced in supernovae, the same mechanism described above could be applied to eliminate implanted Ne. In novae, there are no observations or simulations of the interaction between the nova ejecta and the ISM. Thus, our present knowledge precludes us from determining whether the same mechanism as in supernovae can be applied for the grains formed in nova ejecta.

4. SUMMARY

Presolar graphite carries a ^{22}Ne-rich component called Ne-E(L). Graphite separates extracted from the Murchison meteorite show a range of density (1.6–2.2 g cm^{-3}). Isotopic and elemental features of graphite depend on density, and so does the source of ^{22}Ne: a dominant source of ^{22}Ne is ^{22}Na, but it is also produced via ^{14}N(α, γ)^{18}F($e^{+}\nu$)^{18}O(α, γ)^{22}Ne. The proportions of ^{22}Ne of the two different origins depend on density.

Revisiting the noble gas data on low-density graphite separates KE1 and KE3 from the Murchison meteorite, we conclude that the ^{22}Ne in low-density graphite grains is solely from the decay of ^{22}Na produced in the O/Ne zone in supernovae, not in novae. The noble gas data also indicate that these grains do not contain implanted Ne. These observations can be explained if, after grains encountered the reverse shock, the grains traveled outward into the H-rich zone and subsequently in the ISM, resulting in the sputtering of the surface layer of the grains.

We are grateful to Takashi Kozasa for discussions on dust formation and evolution in supernova ejecta and in the ISM and Kevin Croat for help to run the SRIM code (http://www.srim.org/). We thank Thomas J. Bernatowicz and an anonymous reviewer for the constructive comments, and Bruce Fegley, Jr. for pointing out the presence of intercalated graphite. This work is supported by NASA grants NNX07AF98G and NNX08AG56G.

REFERENCES

Alaerts, L., Lewis, R. S., Matsuda, J., & Anders, E. 1980, Geochim. Cosmochim. Acta, 44, 189
Amari, S., Anders, E., Virag, A., & Zinner, E. 1990, Nature, 345, 238
Amari, S., Gallino, R., Limongi, M., & Chieffi, A. 2006, in AIP Conf. Ser. 847, Origin of Matter and Evolution of Galaxies, ed. S. Kubono, W. Aoki, T. Kajino, T. Motobayashi, & K. Nomoto (Melville, NY: AIP), 311
Amari, S., Hoppe, P., Zinner, E., & Lewis, R. S. 1992, ApJ, 394, L43
Amari, S., Hoppe, P., Zinner, E., & Lewis, R. S. 1993, Nature, 365, 806
Amari, S., Lewis, R. S., & Anders, E. 1994, Geochim. Cosmochim. Acta, 58, 459
Amari, S., Lewis, R. S., & Anders, E. 1995a, Geochim. Cosmochim. Acta, 59, 1411
Amari, S., Zinner, E., & Lewis, R. S. 1995b, ApJ, 447, L147
Amari, S., Zinner, E., & Lewis, R. S. 1996, ApJ, 470, L101
Anders, E. 1988, in Meteorites and the Early Solar System, ed. J. F. Kerridge & M. S. Matthews (Tucson, AZ: Univ. Arizona Press), 927
Anders, E., & Grevesse, N. 1989, Geochim. Cosmochim. Acta, 53, 197
Bernatowicz, T. J., Amari, S., Zinner, E. K., & Lewis, R. S. 1991, ApJ, 373, L73
Bernatowicz, T. J., Cowsik, R., Gibbons, P. C., Lodders, K., Fegley, B. Jr., Amari, S., & Lewis, R. S. 1996, ApJ, 472, 760
Bernatowicz, T. J., Fraundorf, G., Tang, M., Anders, E., Wopenka, B., Zinner, E., & Fraundorf, P. 1987, Nature, 330, 728
Black, D. C., & Pepin, R. O. 1969, Earth Planet. Sci. Lett., 6, 395

Chieffi, A., & Limongi, M. 2004, ApJ, 608, 405
Clayton, D. D. 1975, Nature, 257, 36
Clayton, D. D., Liu, W., & Dalgarno, A. 1999, Science, 283, 1290
Clayton, D. D., Meyer, B. S., The, L.-S., & El Eid, M. D. 2002, ApJ, 578, L83
Croat, T. K., Bernatowicz, T. J., Amari, S., Messenger, S., & Stadermann, F. J. 2003, Geochim. Cosmochim. Acta, 67, 4705
Dresselhaus, M. S., & Dresselhaus, G. 2002, Adv. Phys., 51, 1
Eberhardt, P. 1974, Earth Planet. Sci. Lett., 24, 182
Eberhardt, P., Jungck, M. H. A., Meier, F. O., & Niederer, F. 1979, ApJ, 234, L169
Eberhardt, P., Jungck, M. H. A., Meier, F. O., & Niederer, F. R. 1981, Geochim. Cosmochim. Acta, 45, 1515
Fransson, C., et al. 2005, ApJ, 622, 991
Gallino, R., Busso, M., Picchio, G., & Raiteri, C. M. 1990, Nature, 348, 298
Heck, P. R., Amari, S., Hoppe, P., Baur, H., Lewis, R., & Wieler, R. 2008, ApJ, submitted
Hohenberg, C. M. 1980, Rev. Sci. Instrum., 51, 1075
Hoppe, P., Amari, S., Zinner, E., & Lewis, R. S. 1995, Geochim. Cosmochim. Acta, 59, 4029
Hoppe, P., Strebel, R., Eberhardt, P., Amari, S., & Lewis, R. S. 2000, Meteorit. Planet. Sci., 35, 1157
José, J., & Hernanz, M. 1998, ApJ, 494, 680
José, J., Hernanz, M., Amari, S., Lodders, K., & Zinner, E. 2004, ApJ, 612, 414
Jungck, M. H. A. 1982, Pure ^{22}Ne in the Meteorite Orgueil (München: E. Reinhardt), 80
Kehm, K., Amari, S., Hohenberg, C., & Lewis, R. S. 1996, Lunar Planet. Sci., 27, 657
Klay, N., & Käppeler, F. 1988, Phys. Rev., C 38, 295
Lewis, R. S., Amari, S., & Anders, E. 1990, Nature, 348, 293
Lewis, R. S., Amari, S., & Anders, E. 1994, Geochim. Cosmochim. Acta, 58, 471
Lewis, R. S., Srinivasan, B., & Anders, E. 1975, Science, 190, 1251
Lewis, R. S., Tang, M., Wacker, J. F., Anders, E., & Steel, E. 1987, Nature, 326, 160
Marhas, K. K., Amari, S., Gyngard, F., Zinner, E., & Gallino, R. 2008, ApJ, 689, 622
McCray, R. 1993, ARA&A, 31, 175
Meyer, B. S., Weaver, T. A., & Woosley, S. E. 1995, Meteoritics, 30, 325
Nichols, R. H. Jr., Hohenberg, C. M., Hoppe, P., Amari, S., & Lewis, R. S. 1992, Lunar Planet. Sci., 23, 989
Nichols, R. H. Jr., Kehm, K., Brazzle, R., Amari, S., Hohenberg, C. M., & Lewis, R. S. 1994, Meteoritics, 29, 510
Nittler, L. R., et al. 1995, ApJ, 453, L25
Nozawa, T., Kozasa, T., Habe, A., Dwek, E., Umeda, H., Tominaga, N., Maeda, K., & Nomoto, K. 2007, ApJ, 666, 955
Rauscher, T., Heger, A., Hoffman, R. D., & Woosley, S. E. 2002, ApJ, 576, 323
Rho, J., et al. 2008, ApJ, 673, 271
Rudnick, L. 2008, in AIP Conf. Ser. 1016 Origin of Matter and Evolution of Galaxies, ed. T. Suda, T. Nozawa, A. Ohnishi, K. Kato, M. U. Fujimoto, T. Kajino, & S. Kubono (Melville, NY: AIP), 353
Srinivasan, B., & Anders, E. 1978, Science, 201, 51
Tang, M., & Anders, E. 1988, Geochim. Cosmochim. Acta, 52, 1235
Travaglio, C., Gallino, R., Amari, S., Zinner, E., Woosley, S., & Lewis, R. S. 1999, ApJ, 510, 325
Woosley, S. E., & Weaver, T. A. 1995, ApJS, 101, 181